Dual-Band Circularly Polarized Equilateral Triangular-Patch Array Antenna for Mobile Satellite Communications

Josaphat Tetuko Sri Sumantyo, *Member, IEEE*, Koichi Ito, *Fellow, IEEE*, and Masaharu Takahashi, *Senior Member, IEEE*

***Abstract*—The Japan Aerospace Exploration Agency will launch the Engineering Test Satellite VIII (ETS-VIII) in 2006 to support the next generation of mobile satellite communications covering the area of Japan (beam coverage $El = 38°$ to 58°). In this paper, a satellite-tracking left-handed circularly polarized triangular-patch array antenna is developed for ground applications. The targeted minimum gain of the antenna is set to 5 dBic at the central elevation angle ($El = 48°$), in the Tokyo area, for applications using data transfer of around a hundred kbps. The antenna is composed of three equilateral triangular patches for both reception and transmission units operating at 2.50 and 2.65 GHz frequency bands, respectively. The antenna was simulated by method of moments (MoM) analysis, and measurement of the fabricated antenna was performed to confirm the simulation results. The measurement results show that the frequency characteristics and the 5-dBic gain coverage in the conical-cut plane of the fabricated antenna satisfy the specifications for ETS-VIII. A prototype of the proposed antenna system is employed in outdoor experiments using a pseudosatellite and shows good performance from $El = 38°$ to 58 °.**

***Index Terms*—Circular polarization, dual band, equilateral triangular-patch, mobile satellite communications, outdoor experiments, pseudosatellite.**

I. Introduction

THE Japan Aerospace Exploration Agency (JAXA) will launch a geostationary satellite called Engineering Test Satellite VIII (ETS-VIII) in 2006. ETS-VIII will conduct orbital experiments on mobile satellite communications in the *S*-band frequency range. Mainly in support of the development of a technology for the transmission and reception of multimedia information such as voice and images for land mobile systems [1]. Up to now, various antennas have been developed for mobile satellite communications purposes [2]–[5], but these antennas have a complex composition. In this paper, a low profile dual-band satellite-tracking triangular-patch array antenna is proposed.

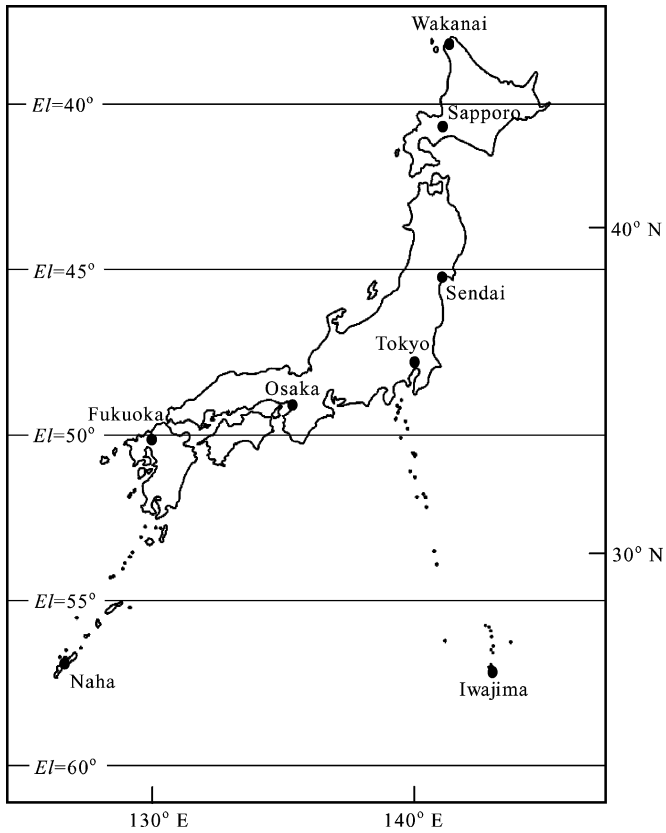

Fig. 1. Japan map: elevation angle of beam direction.

Fig. 1 shows the direction of ETS-VIII seen in Japan that is illustrated by the elevation angle (El). This figure shows that the El of the beam of the developed antenna must cover from 38° (Wakanai city at Hokkaido island) to 58° (Naha city at Okinawa island) to maintain the multimedia service over all of Japan.

The targeted minimum gain of the antenna is set to 5 dBic at the central elevation angle ($El = 48°$) in the Tokyo area for data transfer applications of around one hundred kbps. The antenna should be designed as thin, compact, small, and simple as possible, to allow it to be incorporated onto a car roof [6].

II. Specifications and Targets

Table I shows the specifications and targets desired from an antenna for use with mobile satellite communications, in partic-

Manuscript received December 15, 2004; revised May 12, 2005. This work was supported by the Japan Society for the Promotion of Science (JSPS) Grant-in-Aid for Scientific Research under Project 16360185.

J. T. S. Sumantyo was with Center for Frontier Electronics and Photonics, Chiba University, Inage, Chiba 263-8522 Japan. He is now with the Center for Environmental Remote Sensing, Chiba University, Inage, Chiba 263-8522 Japan, and the Remote Sensing Research Center, Pandhito Panji Foundation, Bandung 40191 Indonesia (e-mail: jtetukoss@faculty.chiba-u.jp; tetuko@pandhitopanji-f.org).

K. Ito and M. Takahashi are with the Research Center for Frontier Medical Engineering, Inage, Chiba 263-8522 Japan (e-mail: ito.koichi@faculty.chiba-u.jp).

Digital Object Identifier 10.1109/TAP.2005.858849

TABLE I
SPECIFICATIONS ON THE ANTENNA FOR MOBILE SATELLITE COMMUNICATIONS (ETS-VIII)

SPECIFICATIONS		
frequency bands	transmission (Tx)	2655.5 to 2658.0 MHz
	reception (Rx)	2500.5 to 2503.0 MHz
polarization	Left-Handed Circular Polarization (LHCP) for both transmission and reception	
TARGETS		
elevation angle (El)		48° (Tokyo) ± 10°
azimuth angle (Az)		0° to 360°
minimum gain		5 dBic
maximum axial ratio		3 dB
maximum isolation		20 dB

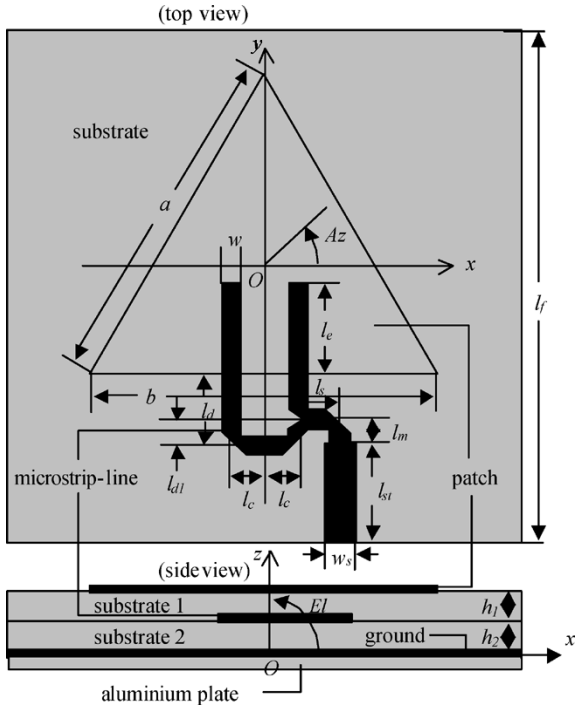

Fig. 2. Configuration of single triangular patch antenna.

ular aimed at ETS-VIII applications, that are used in this paper. In this paper, the operating frequency of a single patch for reception (Rx) and transmission (Tx) are set to 2.5025 and 2.6575 GHz, respectively, as shown in Table I. Both Rx and Tx are considered to work in left-handed circular polarization (LHCP) where the maximum axial ratio is 3 dB in the targeted direction (azimuth angle $Az = 0°$ to 360° and $El = 48°$).

III. ANTENNA CONFIGURATION

The antenna as single patch is discussed prior to the consideration of the array configuration. Fig. 2 shows the configuration of a single equilateral triangular-patch with its parameters. The antenna is fabricated using a conventional substrate (relative permittivity $\varepsilon_r = 2.17$ and $\tan\delta = 0.000\,85$). The elements are fed by novel type of proximity feeds with microstrip-lines whose widths w are 3.0 mm for each patch of Rx and Tx to obtain a thin configuration. A novel dual feed type is proposed for the generation of left-handed circular polarization (LHCP) by using equilateral triangular-patch, where one of the microstrip-line feeds is $\lambda/4$ longer than the other introducing a 90° phase delay. In the same manner, a right-handed circular polarization (RHCP) could be realized by swapping the microstrip-lines. The proposed feeding technique is designed to obtain an ideal and stable current distribution on the triangular-patch surface hence improving previously developed antennas [7], [8].

Several types of previous circularly polarized triangular antennas have been developed [9]–[13], but they are difficult to design and optimize, because the ratio between a and b (see Fig. 2) affects the performance of the axial ratio with a high degree of sensitivity. The probe feed technique is commonly applied to generate a circularly polarized triangular patch antenna, but this technique is more complicated than the microstrip-line or proximity feed technique in the fabrication process. Additionally, the probe feeding technique with a single feeding point, will generate an unstable current distribution on each patch when the patches are composed in an array configuration. Therefore, by using a proposed microstrip-line for equilateral triangular-patches as shown in Fig. 2, the design and fabrication of the antennas is made easier, without the need to optimize the ratio between a and b.

In this paper, the method of moment (MoM)(IE3D Zeland software) was employed to simulate the model with a finite ground plane. Consideration of the efficient thickness of the antenna (see Fig. 2) allowed either the substrate thickness for the microstrip-line or feeding line (substrate 2) and triangular patch (substrate 1) to be defined with the other implicit ($h_1 = h_2 = 0.8\,\mathrm{mm}$). The lengths of microstrip-line inserted under the patch l_e are 14 and 10 mm for Rx and Tx, respectively and a quarter-wave transformer is used to obtain a matching impedance of 50 Ω for Rx and Tx, respectively. The microstrip-lines are fed using an SMA connector on the edge of the substrate. The detailed parameters of the microstrip-line (see Fig. 2) for Rx and Tx are $l_s = 5\,\mathrm{mm}$, $l_d = 11\,\mathrm{mm}$, $l_{d1} = 4\,\mathrm{mm}$, $l_c = 5\,\mathrm{mm}$, $l_m = 2\,\mathrm{mm}$, and $l_{st} = 11\,\mathrm{mm}$. The width of the input microstrip-line w_s for Rx and Tx are 4.7 mm and 4.0 mm, respectively. The patch lengths are independently optimized for the specifications of either Rx or Tx by using a single patch. The patch length parameters (for $a = b$) obtained are 52.5 and 49.4 mm for Rx and Tx, respectively.

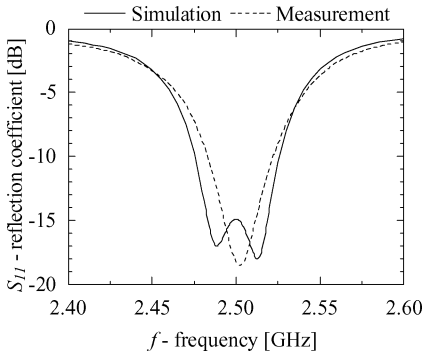

Fig. 3. Reflection coefficient versus frequency of single triangular patch antenna (reception).

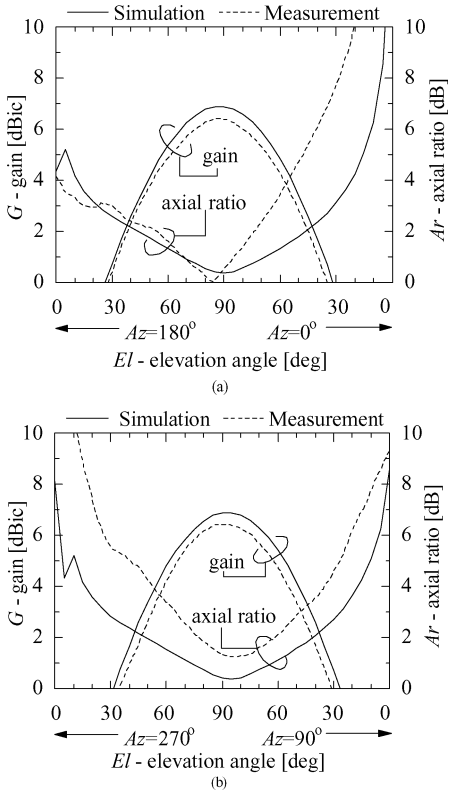

Fig. 4. Radiation pattern (reception). (a) $Az = 0°$. (b) $Az = 90°$.

Fig. 3 shows the relationship between the reflection coefficient (S_{11}) and frequency for the simulation model and the fabricated Rx antenna. The characteristic of the Tx antenna can be simulated and fabricated in the same manner and therefore is neglected in this discussion. From this Fig. 3, it can be seen that by comparison of the measurement to the simulation there is a high degree of agreement at the center frequency, however, they show a 0.4% difference in -10 dB bandwidth. This bandwidth difference is due to fabrication errors (e.g., drilling error about 0.1 mm) and the influence of the measurement system (connector, aluminum plate, etc.).

Fig. 4(a) and (b) depicts the relationship between gain (G) and El at an azimuth angle $Az = 0°$ and 90°, respectively. From Fig. 4(a) the 5 dBic-gain beamwidth by simulation and measurement are 60° and 52°. From this figure, the maximum gain obtained from the measurements is 0.45 dB lower than the

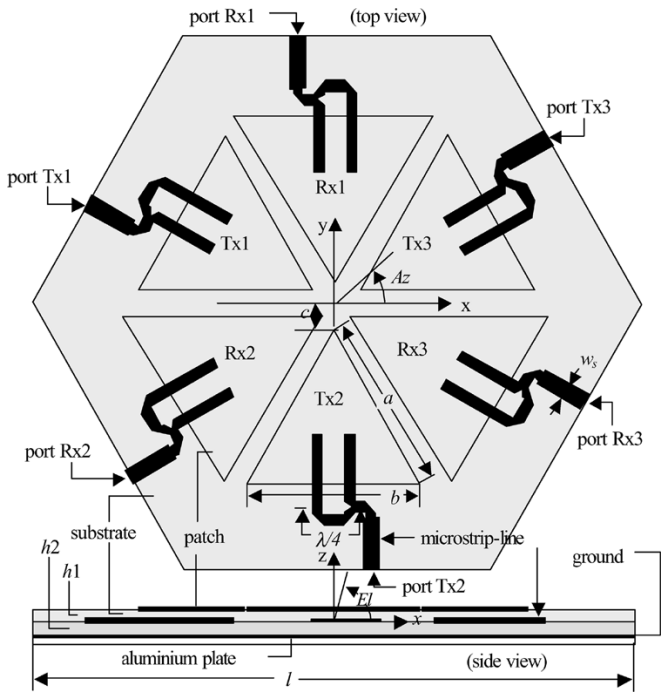

Fig. 5. Dual-band equilateral triangular-patch array antenna.

simulation results. This is due to the various losses that occur during the measurement. This result shows that a finite ground plane strongly affects the radiation pattern, especially the axial ratio (Ar) characteristics. The configuration of an antenna and the measurement system, i.e., the coaxial cable, the connector, the hole, and the plastic screws in the substrates, etc., are also considered to affect the current distribution on the surface of the patches, therefore decreasing the Ar performance. From Fig. 4(b), the 5 dBic-gain beamwidth of the simulation and measurement are 60° and 52°, respectively. From the same figure, the maximum gain obtained from the measurements is 0.45 dB lower than that of the simulation. The same features as observed in Fig. 4(a) occur and the same explanations can be applied.

Considering only the simulation results, the size of the Rx patch that uses the proposed feeding type is 0.6% larger than the previous type of patch ($a = 52.1$ mm and $b = 53.0$ mm) which is fed by a probe as discussed in [11], [12] when applied to the *S*-band frequency. The maximum gain of the proposed antenna is 0.2 dB higher than the previous one. However, the 5-dBic-gain beamwidth of the proposed antenna at azimuth angle $Az = 0°$ and 90° is 10.0% and 4.5% narrower than the previous antenna, respectively. This result shows that the enlargement of the patch size increases the maximum gain and reduces the beamwidth. Additionally, the 3-dB-axial ratio beamwidth of the proposed antenna at azimuth angle $Az = 0°$ and 90° is 25.0% and 11.8% wider than the previous type, respectively. This result shows the proposed antenna is greatly improved in terms of axial ratio which is a very important characteristic for circularly polarized antennas.

Fig. 5 shows the configuration of the triangular-patch array antenna; the Tx and Rx sections are composed of three triangular elements each. This configuration is used to minimize space usage. The fabricated triangular-patch array antenna is

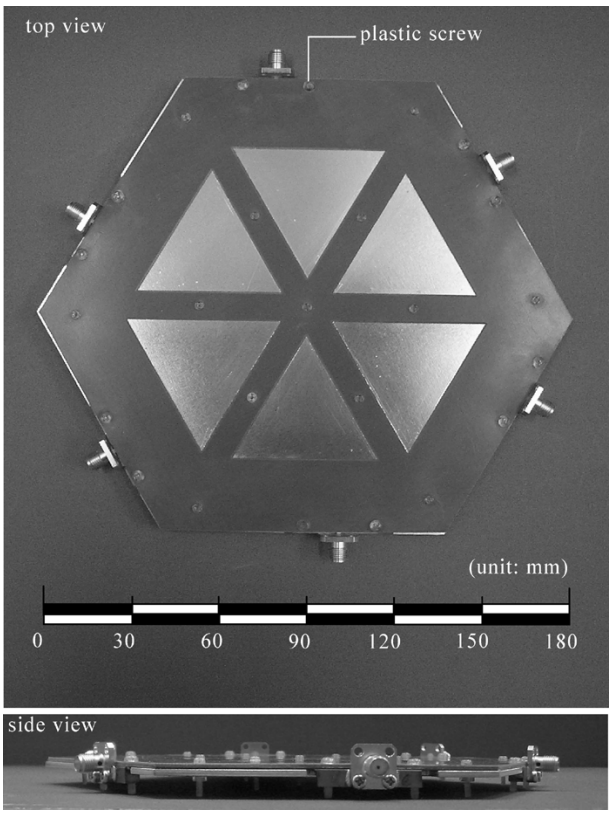

Fig. 6. Fabricated antenna.

shown in Fig. 6 from the top and side. An aluminum plate with thickness 2 mm is used to support the substrate.

The characteristics of the antenna in this array configuration are discussed in terms of the influence of the distance between the patch apex and the center of the array (c), (refer to Fig. 5). In consideration of the target size of the antenna defined in Table I, c is varied from 2 to 20 mm. This paper offers a discussion of the antenna's reception only, with the transmission deducible in the same manner.

Fig. 7(a) shows the relationship between G and Az for $c = 2$, 10, and 20 mm at $El = 48°$. The simulated results shows that the 5-dBic beamwidths for $c = 2$, 10, and 20 mm are 120°, 130°, and 130°, respectively. The saddle shape in the beam, shown in Fig. 7(a), influences the antenna gain over the main beam, which is inversely proportional to c. The saddle shape is generated by patches that are turned-on with a large distance between them. This figure also shows that increasing c results in an increase in side lobe level. The beamwidth target is satisfied for all three lengths of c, i.e., greater than 120°, covering the whole azimuth angle.

Fig. 7(b) shows the relationship between Ar and Az. This figure shows that the 3-dB axial ratio beamwidths are 110°, 140°, and 130° when $c = 2$, 10, and 20 mm, respectively. This result highlights that the 3-dB axial ratio beamwidth for $c = 10\,\mathrm{mm}$ provides the widest coverage. In the case of $c = 20\,\mathrm{mm}$, the axial ratio beamwidth is shifted in comparison to the 5-dBic gain beamwidth that is shown in Fig. 7(a). This shifting is considered to be due to the affects of decreasing the gain in Fig. 7(a).

Based on the aforementioned results, the distance of the patch apex to the center of the antenna (c) is selected as 10 mm. This

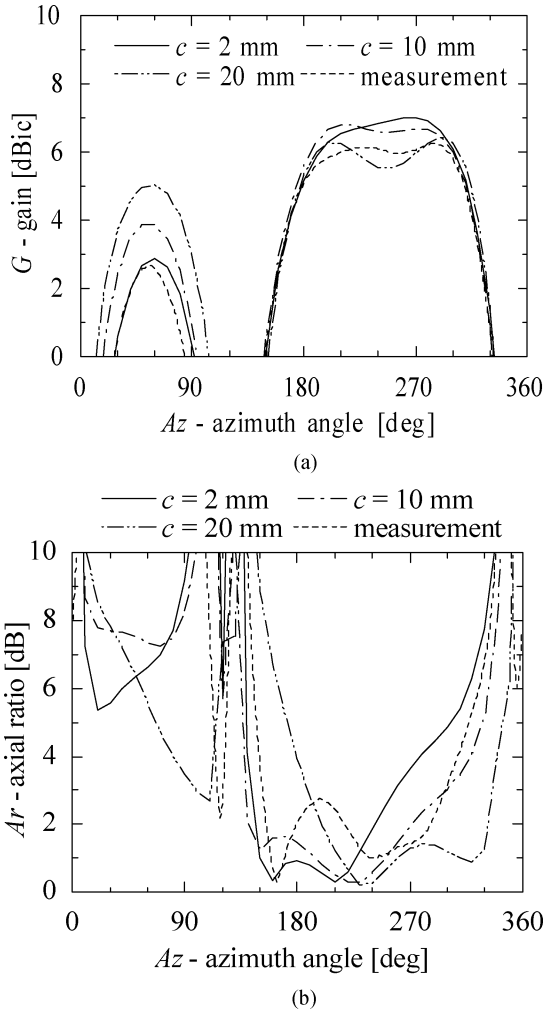

Fig. 7. Array antenna characteristic in azimuth angle (reception). (a) Gain versus azimuth angle ($El = 48°$). (b) Axial ratio versus azimuth angle ($El = 48°$).

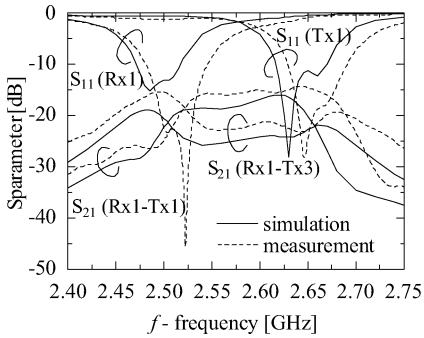

Fig. 8. S-parameter versus frequency.

means that the diameter of the model l is set to 190 mm. The performance of the antenna in a dual-band configuration will be discussed next.

IV. Performance of the Antenna

Fig. 8 shows the S-parameters obtained from the simulation model and the measurement for element no. 1 of the Rx and Tx, shown in Fig. 5 as Rx1 and Tx1. This figure shows that the simulation results for both Rx and Tx are shifted 0.7% and 0.5%,

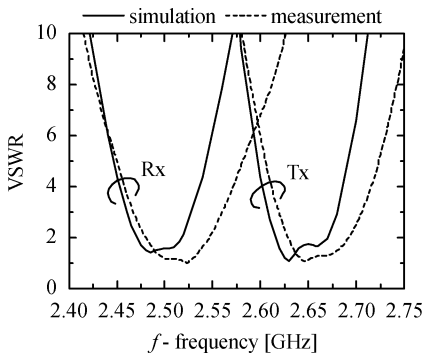

Fig. 9. VSWR versus frequency.

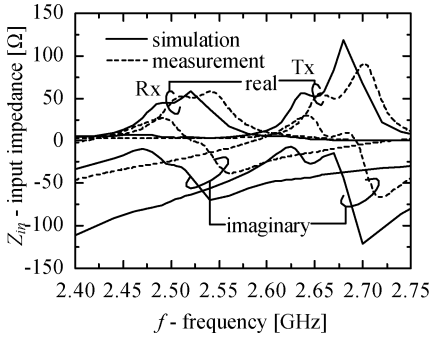

Fig. 10. Input impedance versus frequency.

respectively, to lower frequencies from the measurement result. It is considered that the measurement systems (i.e., cable, connectors, plastic screws, etc.) affect the characteristics of the antenna. This figure shows that the measurement result for each Rx and Tx patch have sufficient bandwidth to cover the frequency bands shown in Table I. Then the isolation of the closest patches (e.g., Rx1 to Tx1 and Rx1 to Tx3 in Fig. 5), is higher than 15 dB. This result is less that the target due to the small distance between Rx and Tx, which generates significant coupling between adjacent patches, which in turn affects the isolation. Fig. 9 shows the VSWR of Rx1 and Tx1. From this graph, the measurement result is seen to satisfy the targets set in Table I. This figure also shows that the simulation results of Rx and Tx are shifted by 0.7% and 0.5%, respectively, lower frequencies in comparison to the measurement.

Fig. 10 shows the input impedance characteristics of patch Rx1 and Tx1. This figure also shows the simulation results are shifted to lower frequencies from the measured results by 0.7%. The real part of measurement at the Rx and Tx target frequencies (center frequency of Rx 2.5025 GHz and Tx 2.6575 GHz) is 50 Ω providing a good match.

V. Beam–Switching Technique

A. Beam Generation

The beam of the antenna is generated by a simple mechanism that consists of switching OFF one of the radiating elements shown in Fig. 5. By considering the mutual coupling between fed elements, their phase and distance, the beam direction can be varied. Hence, the two fed elements theoretically generate a beam shift of -90° in the conical-cut direction from the element that is switched OFF, in the case of a LHCP antenna. For

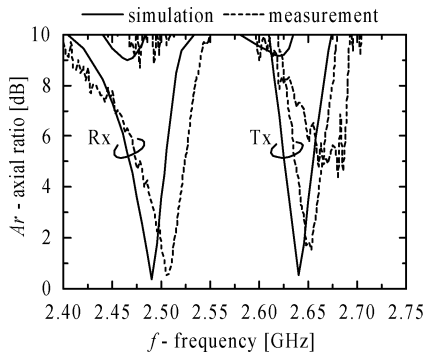

Fig. 11. Axial ratio versus frequency.

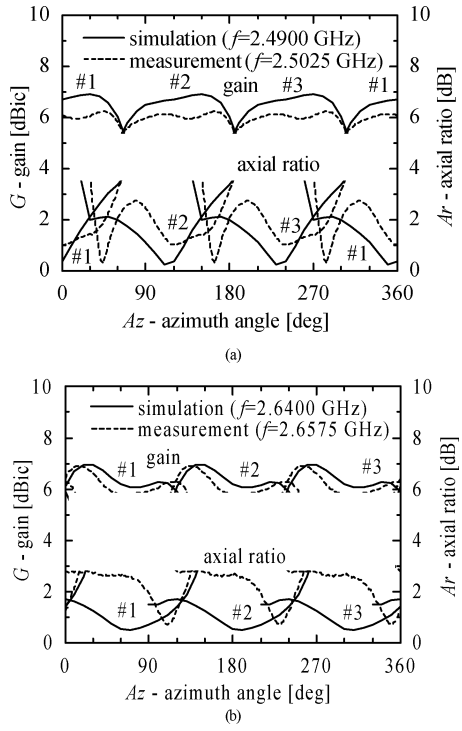

Fig. 12. Radiation characteristics in the conical-cut plane for an elevation angle $El = 48^\circ$. (a) Reception. (b) Transmission.

example, when Rx element 3 placed at $Az = 330^\circ$ is switched OFF, the beam is theoretically directed toward the azimuth angle $Az = 240^\circ$ (see Fig. 12, beam no. 3 shown as symbol #3 in the graph). The other two beams of reception can be generated in the same manner, switching each element OFF successively (Rx2 and Rx3 in Fig. 5 and each beam shown as symbol #2 and #3 in Fig. 12, respectively).

The antenna characteristics are defined by the axial ratio characteristics at $El = 48^\circ$ when Rx3 and Tx3 are switched OFF. The main beams of Rx and Tx are directed to $Az = 240^\circ$ and 300°, respectively. The azimuth angle is chosen by considering the direction of the main beam of the antenna, in the case where Rx3 and Tx3 are switched OFF (see also Fig. 12). Based on the simulation and measurement results as shown in Fig. 11, the minimum axial ratio of Rx and Tx obtained are 0.35 and 0.54 dB at 2.4900 and 2.6400 GHz for simulation, and 0.56 and 1.52 dB at 2.5075 and 2.6525 GHz for measurement. The axial ratio of the measurement result at frequencies of 2.5025 and 2.6575

GHz are 1.08 and 2.8 dB, respectively. The measurement results show that the axial ratio characteristics satisfy the targeted performance of the frequency band. The simulation results shows the minimum axial ratios of antenna are shifted to lower frequencies by 0.7% and 0.5% of the measurement result. This is considered to be due to the effect of the ground plane size, the hole in the substrate, connector, and coaxial cables, etc. The frequency of the minimum axial ratio achieved by simulation and measurement are used to derive the antenna performance as discussed next.

B. Verification of Beam Switching

The simulation and measurement results of gain and axial ratio characteristics of the beam switching in the conical-cut plane are shown in Fig. 12(a) and (b) for Rx and Tx, respectively. The figures show that the maximum gain is 5.4 dBic for both the simulation and the measurement of Rx, and 5.9 dBic and 5.8 dBic for both the simulation and measurement of Tx. From these results, both simulation and measurement results are better than the targets in Table I (minimum gain 5.0 dBic) and cover the whole azimuth angle (the 5-dBic beam coverage is more than 120°).

The minimum axial ratios obtained from the simulation and measurement of Rx are both 3.4 dB, as shown in Fig. 12(a). The 3-dB axial ratio coverage of the simulation and measurement results cover 351° in the conical-cut plane at $El = 48°$. Although this does not yet satisfy the target empirically, this antenna works very well in an outdoor environment as explained later. Then Fig. 12(b) shows that the minimum axial ratio for the simulation and measurement of Tx are 1.7 and 2.8 dB, respectively. The 3-dB axial ratio coverage of the simulation and measurement results covers 360° in the conical-cut plane at $El = 48°$.

The measurement results of Rx and Tx (Fig. 12) show a saddle-shape scalloping occurs for both the main beam gain and axial ratio. The scalloping in the main beam becomes more apparent when the distance between the center of the antenna and the apex of patch is reduced [8] or the distance decreased. This effect is also considered to decrease the performance of the antenna, especially its axial ratio. This is due to the influence of the edge effect that generates an oscillation of current distribution on the surface of the patch with finite ground plane and the change in antenna characteristics as the substrate surface is reduced, in particular the resonant frequency (see Fig. 3) and radiation pattern [14]–[20].

Fig. 13(a) and (b) shows the radiation characteristics in the elevation-cut for Rx and Tx, respectively. If the antenna is put on the car roof and must cover the area of Japan (see Fig. 1), considered to be ±10° in elevation with center at $El = 48°$, the gain and axial ratio in this range must satisfy the targets (minimum gain 5 dBic and maximum axial ratio 3 dB).

Fig. 13(a) shows that the gain of simulation result, between $El = 40°$ and 58° is higher than 5 dBic, and the measurement result can cover from $El = 42°$ to 58°. The axial ratio of both simulation and measurement from $El = 38°$ to 58° are lower than 3 dB, showing that the axial ratio of Rx satisfies the targets. At this point the gain at low elevation angles needs to be improved by around 2° and 4° for simulation and measurement respectively, to meet the desired targets.

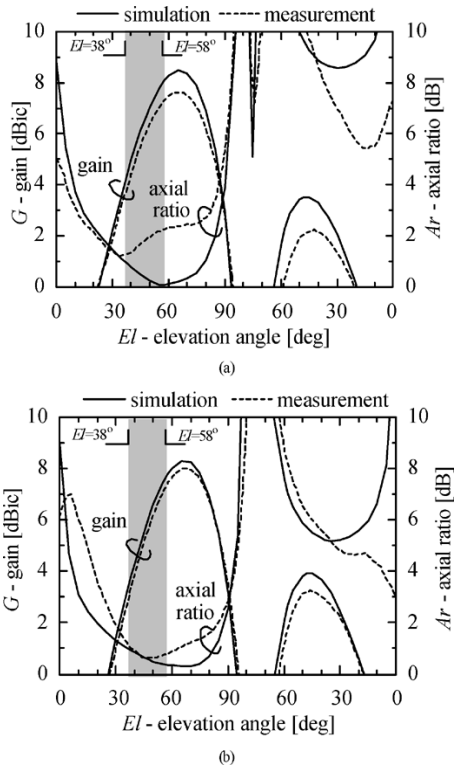

Fig. 13. Radiation characteristics in the elevation-cut. (a) Reception. (b) Transmission.

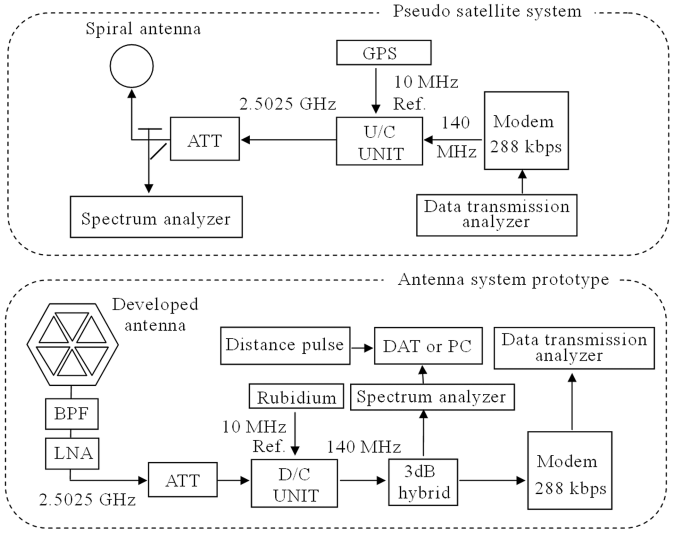

Fig. 14. Prototype of antenna system and pseudosatellite system.

Fig. 13(b) shows the gain of the simulation result, between $El = 43°$ and 58° is higher than 5 dBic, and the measurement result can cover from $El = 45°$ to 58°. The axial ratio of both simulation and measurement from $El = 38°$ to 58° are lower than 3 dB, showing that the axial ratio of Tx satisfies the targets. At this point, the gain at low elevation angles needs to be improved by around 5° and 7° for simulation and measurement respectively, to meet the desired targets.

TABLE II
FORWARD-LINK BUDGET FOR PSEUDOSATELLITE EXPERIMENT

	Units	Forward-link budget for ETS-VIII	Forward-link budget for pseudo satellite (El=48°)
Frequency	GHz	2.5025	2.5025
Output power (transmission)	dBW	16.99	-43.15
Feeder loss	dB	1.00	17.75
Antenna gain	dBi	41.00	0.16
EIRP transmission	dBW	56.99	-60.74
Distance between experiment car and satellite	km	37207.83	0.041
Propagation loss	dB	191.8	72.65 (simulation value)
Polarization loss	dB	0.2	
Fading margin	dB	2.50	
G/T (measurement result at El=48°)	dB/K	-19.41	-19.41
C/N_0 reception	dBHz	71.70	75.50

VI. ANTENNA SYSTEM PROTOTYPE AND OUTDOOR EXPERIMENT USING A PSEUDOSATELLITE

A. Prototype of Antenna System and Pseudosatellite System

In this paper, outdoor experiments were held to investigate the propagation characteristics of the antenna developed and a pseudosatellite system. Fig. 14 shows the prototype of the antenna system and the pseudosatellite system.

The antenna employed in the prototype antenna system is the developed dual-band equilateral triangular-patch array antenna. Due to the restricted frequency licence, only the reception (downlink) was investigated. As shown in Fig. 14, the antenna is connected to a bandpass filter (BPF), because the antenna operating frequency (2.5025 GHz) is close to that of wireless LANs. It is connected serially to a low-noise amplifier (LNA) and an attenuator (ATT). The downconverter (D/C) unit is employed to obtain data at a frequency of 140 MHz readable by a spectrum analyzer and a modem (288 kbps). The rubidium frequency (10 MHz) is used by the D/C unit as a reference. The data read by the spectrum analyzer can be recorded by a DAT storage system (DAT) or personal computer (PC). The distance pulse is used to acquire the position of the experiment car whose data is simultaneously recorded by the spectrum analyzer. The output data of the modem are displayed and recorded by the data transmission analyzer. The prototype of the antenna system is installed on the experiment car as shown in Fig. 15.

The pseudosatellite system, also shown in Fig. 14, is composed of a data transmission analyzer and a modem (288 kbps) with an output frequency of 140 MHz. This frequency is converted to 2.5025 GHz by an upconverter (U/C) unit. The U/C unit uses the GPS frequency (10 MHz) as a reference and the output is connected to an attenuator (ATT) to adjust the output intensity of a spiral antenna to be same as the output of ETS-VIII (refer to the forward-link budget as shown in Table II).

B. Outdoor Experiments and Result

Fig. 15 shows the situation of the outdoor experiments. The pseudosatellite system mounted on the building roof, whose height is 33 m from the ground. The direction of the main beam

Fig. 15. Outdoor experiments.

of the spiral antenna is installed with an elevation angle of 48° to the ground to simulate the beam direction of ETS-VIII. The forward-link budget of the pseudosatellite is simulated to be the same as the forward-link budget of ETS-VIII (see Table II).

The developed antenna system is mounted on the car roof on top of an aluminum plate (40 cm × 40 cm) for support. It is then covered by a radome to avoid the effects environmental influences (wind, dust, rain water, etc.) during the experiment. Patch Rx1 of the installed antenna is turned OFF to generate the beam. The car is set in three positions so that the main beam direction of the antenna is $El = 38°$, $El = 48°$ and $El = 58°$ from the pseudosatellite position and the Rx radiation pattern is recorded at a frequency of 2.5025 GHz, shown in Fig. 16 [21]. The low elevation angle ($El = 38°$) and high elevation angle ($El = 58°$) are used to simulate the antenna performance at Wanakai city and Naha city. The measurement results are seen

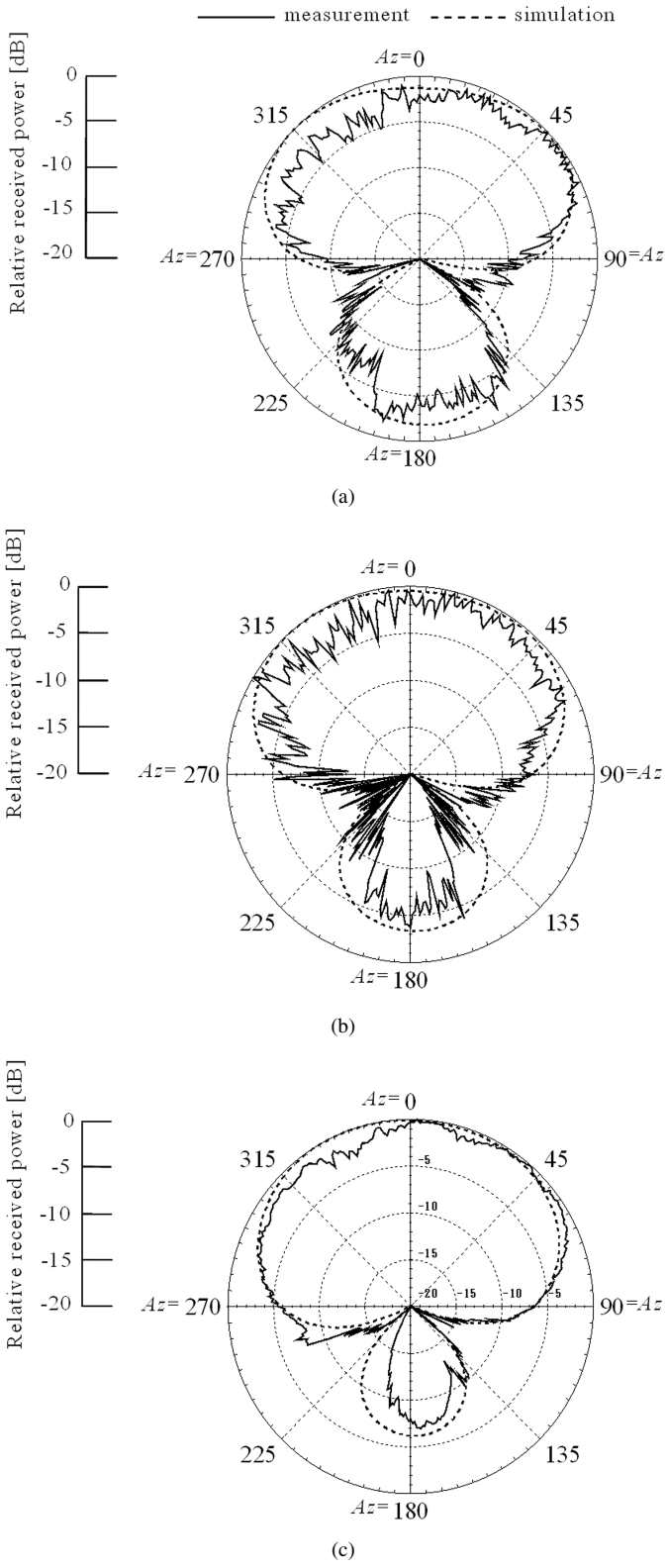

Fig. 16. Relative received power (reception) at $El = 38°, 48°, 58°$.

to compare well with the simulation results, where the simulation results are calculated using the MoM. The scalloping in the measurements is caused by the influence of the car roof. The effect of the surrounding environment for example reflections from buildings can also be considered to give rise to the occurrence of scalloping.

VII. Conclusion

JAXA will launch ETS-VIII in 2006 to conduct orbital experiments on mobile satellite communications in the *S*-band. A circularly polarized satellite-tracking dual-band equilateral triangular-patch array antenna for mobile satellite communications aimed at ETS-VIII applications has been developed in this paper. The MoM was employed in the design of the antenna and measurement of a fabricated antenna was performed to confirm the simulation results.

The antenna developed is thin, small, simple, and compact in comparison to previous antenna designs. The design offers stable switching, able to generate beams that can cover the azimuth angles desired for such an antenna in both Rx and Tx. The measurement results show that the frequency characteristics and the 5-dBic gain coverage in the conical-cut plane of the fabricated antenna satisfy the specifications of ETS-VIII at an elevation of 48°. Outdoor experiments using the antenna and its prototype system were conducted using a pseudosatellite. The measured radiation patterns match well with the simulation results obtained.

Following on from this paper, the dual-band antenna will be developed to improve its performance at low elevation angles. Moreover the antenna will be employed in outdoor experiments in the Tokyo area (central beam direction: $El = 48°$) using ETS-VIII once launched.

Acknowledgment

The authors would like to thank the National Institute of Information and Communications Technology – NICT (former Communication Research Laboratory – CRL), Japan, for their joint research in the outdoor measurements.

References

[1] J. H. Jang, M. Tanaka, and N. Hamamoto, "Portable and deployable antenna for ETS-VIII," in *Proc. Interim Int. Symp. Antennas and Propagation*, 2002, pp. 49–52.

[2] K. Ito, K. Ohmaru, and Y. Konishi, "Planar antennas for satellite reception," *IEEE Trans. Broadcast.*, vol. 34, no. 4, pp. 457–464, Dec. 1988.

[3] K. Ito, J.-P. Daniel, and J.-M. Lenormand, "A printed antenna composed of strip dipoles and slots generating circularly polarized conical patterns," in *Proc. IEEE AP-S Int. Symp.*, 1989, pp. 632–635.

[4] K. Fujimoto and J. R. James, *Mobile Antenna Systems Handbook*. Boston, MA: Artech House, 1994.

[5] M. Nakano, H. Arai, W. Chujo, M. Fujise, and N. Goto, "Feed circuits of double-layered self-diplexing antenna for mobile satellite communications," *IEEE Trans. Antennas Propag.*, vol. 40, no. 10, pp. 1269–1271, Oct. 1992.

[6] H. Ishihara, A. Yamamoto, and K. Ogawa, "A simple model for calculating the radiation patterns of antennas mounted on a vehicle roof," in *Proc. Interim Int. Symp. Antenna and Propagation*, 2002, pp. 548–551.

[7] J. T. S. Sumantyo and K. Ito, "Simple satellite-tracking triangular-patch array antenna for ETS-III applications," IEICE Tech. Rep., AP2003–236, 2004.

[8] J. T. S. Sumantyo, K. Ito, D. Delaune, T. Tanaka, and H. Yoshimura, "Simple satellite-tracking dual-band triangular-patch array antenna for ETS-VIII applications," in *Proc. IEEE Int. Symp. Antennas and Propagation*, 2004, pp. 2500–2503.

[9] J. H. Lu and K. L. Wong, "Singly-fed circularly polarized equilateral-triangular microstrip antenna with a tuning stub," *IEEE Trans. Antennas Propag.*, vol. 48, no. 12, pp. 1869–1872, Dec. 2002.

[10] Y. Suzuki, N. Miyano, and T. Chiba, "Circularly polarized radiation from singly-fed equilateral-triangular microstrip antenna," *Proc. Inst. Elect. Eng.*, pt. H, vol. 134, no. 2, pp. 194–198, Apr. 1987.

[11] R. Garg, P. Bhartia, I. Bahl, and A. Ittipiboon, *Microstrip Antenna Design Handbook*. Boston, MA: Artech House, 2001.
[12] J. R. James and P. S. Hall, *Handbook of Microstrip Antennas*. London, U.K.: Peter Peregrinus, 1989.
[13] G. Kumar and K. P. Ray, *Broadband Microstrip Antennas*. Boston, MA: Artech House, 2003.
[14] J. T. S. Sumantyo, K. Ito, D. Delaune, T. Tanaka, T. Onishi, and H. Yoshimura, "Numerical analysis of ground plane size effects on patch array antenna characteristics for mobile satellite communications," *Int. J. Numer. Modeling*, vol. 18, no. 2, pp. 95–106, Mar./Apr. 2005.
[15] M. F. Otero and R. G. Rojas, "Analysis and treatment of edge effects on the radiation pattern of a microstrip patch antenna," in *Proc. IEEE AP-S Int. Symp.*, 1995, pp. 1050–1053.
[16] E. Lier and K. Jacobsen, "Rectangular microstrip patch antennas with infinite and finite ground plane dimensions," *IEEE Trans. Antennas Propag.*, vol. 31, no. 6, pp. 978–984, Nov. 1983.
[17] H. J. Delgado, J. T. Williams, and S. A. Long, "Substraction of edge-diffracted fields in antenna radiation pattern for simulation of infinite ground plane," *Electron. Lett.*, vol. 25, no. 11, pp. 694–696, May 1989.
[18] S. M. V. Iyer and R. N. Karekar, "Edge effects for resonance frequency of covered rectangular microstrip patch antenna," *Electron. Lett.*, vol. 27, no. 17, pp. 1509–1511, Aug. 1991.
[19] S. Maci and L. Borselli, "Diffraction at the edge of a truncated grounded dielectric slab," *IEEE Trans. Antennas Propag.*, vol. 44, no. 6, pp. 863–873, Jun. 1996.
[20] S. Maci, L. Borselli, and A. Cucurachi, "Diffraction from a truncated grounded dielectric slab: A comparative full-wave/physical-optics analysis," *IEEE Trans. Antennas Propag.*, vol. 48, no. 1, pp. 48–57, Jan. 2000.
[21] S. Ohmori, H. Wakana, and S. Kawase, *Mobile Satellite Communications*. London, U.K.: Artech House, 1998.

Josaphat Tetuko Sri Sumantyo (S'00–A'02–M'04) was born in Bandung, Indonesia, on June 25, 1970. He received the B.Eng. and M.Eng. degrees in electrical and computer engineering (ground penetrating radar systems) from Kanazawa University, Japan, in 1995 and 1997, respectively, and the Ph.D. degree in artificial system sciences (applied radio wave and radar systems) from Chiba University, Chiba, Japan, in 2002.

From 1990 to 1999, he was a Researcher with the Indonesian Governmental Agency for Assessment and Application of Technology (BPPT) and the Indonesian National Army (TNI-AD). In 2000, he was with the Center for Environmental Remote Sensing, Chiba University, as a Research Assistant, and from 2002 to 2005, he was a Lecturer (Postdoctoral Fellowship Researcher) with the Center for Frontier Electronics and Photonics, of the same university. He has been a Director with the Remote Sensing Research Center, Pandhito Panji Foundation, Indonesia (www.pandhitopanji-f.org) since 2000. He is currently an Associate Professor with the Microwave Remote Sensing Laboratory, Center for Environmental Remote Sensing, Chiba University. His main interests include analysis of printed antennas for mobile satellite communications and ultrawide-band synthetic aperture radar (UWB-SAR), scattering wave analysis and its applications in microwave remote sensing. His laboratory is also developing geographical information system for Asian Geospatial Information Database (AGID).

Dr. Sri Sumantyo is a Member of the IEICE, JSPRS, and RSSJ. He is the recipient of many awards and research grants related to his study and research.

Koichi Ito (M'81–SM'02–F'05) was born in Nagoya, Japan, in June 1950. He received the B.S. and M.S. degrees from Chiba University, Chiba, Japan, in 1974 and 1976, respectively, and the D.E. degree from the Tokyo Institute of Technology, Tokyo, Japan, in 1985, all in electrical engineering.

From 1976 to 1979, he was a Research Associate with the Tokyo Institute of Technology. From 1979 to 1989, he was a Research Associate with Chiba University. From 1989 to 1997, he was an Associate Professor with the Department of Electrical and Electronics Engineering, Chiba University, and is currently a Professor with the Research Center for Frontier Medical Engineering, as well as with the Faculty of Engineering, Chiba University. He has been appointed as one of the Vice-Executive Directors for Academic R&D, and Director, Office of Research Administration, Chiba University, since April 2005. In 1989, 1994, and 1998, he was with the University of Rennes I, France, as an Invited Professor. His main interests include analysis and design of printed antennas and small antennas for mobile communications, research on evaluation of the interaction between electromagnetic fields and the human body by use of numerical and experimental phantoms, and microwave antennas for medical applications such as cancer treatment.

Dr. Ito is a member of the AAAS, the IEICE of Japan, the Institute of Image Information and Television Engineers of Japan (ITE), and the Japanese Society of Hyperthermic Oncology. He served as Chair of Technical Group on Radio and Optical Transmissions of ITE from 1997 to 2001. He also served as Chair of the IEEE AP-S Japan Chapter from 2001 to 2002. He is Chair of the Technical Group on Human Phantoms for Electromagnetics, IEICE, Vice-Chair of the 2007 International Symposium on Antennas and Propagation (ISAP2007), and an Associate Editor of the IEEE TRANSACTIONS ON ANTENNAS AND PROPAGATION.

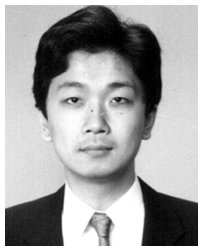

Masaharu Takahashi (M'95–SM'02) was born in Chiba, Japan, on December 15, 1965. He received the B.E. degree in electrical engineering in 1989 from Tohoku University, Miyagi, Japan, and the M.E. and D.E. degrees in electrical engineering from Tokyo Institute of Technology, Tokyo, Japan, in 1991 and 1994, respectively.

He was a Research Associate from 1994 to 1996, an Assistant Professor from 1996 to 2000 with the Musashi Institute of Technology, Tokyo, Japan, and an Associate Professor from 2000 to 2004 with the Tokyo University of Agriculture and Technology. He is currently an Associate Professor with Chiba University, Chiba, Japan. His main interests are electrically small antennas, planar array antennas (RLSA), EMC, and research on evaluation of the interaction between electromagnetic fields and the human body by use of numerical and experimental phantoms.

Dr. Takahashi received the IEEE AP-S Tokyo chapter Young Engineer Award in 1994. He is a member of the IEICE.